



Thermal-stable blue-red dual-emitting $\text{Na}_2\text{Mg}_2\text{Si}_6\text{O}_{15}$: Eu^{2+} , Mn^{2+} phosphor for plant growth lighting

Wanjun Gong^a, Jiabao Luo^b, Weiying Zhou^b, Jiaqi Fan^b, Zishan Sun^b, Senxiang Zeng^b, Haowen Pan^b, Zhenpeng Zhu^c, Xixiao Yang^{a,*}, Zhiqiang Yu^{a,b,**}, Xinguo Zhang^{b,***}

^a Department of Pharmacy, Shenzhen Hospital, Southern Medical University, Shenzhen, 518101, China

^b School of Pharmaceutical Sciences, Southern Medical University, Guangzhou, 510515, China

^c Department of Pharmacy, Guangdong Second Provincial General Hospital, Guangzhou, 510317, China



ARTICLE INFO

Keywords:
Phosphor
Plant growth
LEDs
Energy-transfer

ABSTRACT

Dual-emitting alkaline silicate phosphors $\text{Na}_2\text{Mg}_2\text{Si}_6\text{O}_{15}$: Eu^{2+} , Mn^{2+} have been synthesized to realize blue and red emissions to boost photosynthesis process. At UV excitation, $\text{Na}_2\text{Mg}_2\text{Si}_6\text{O}_{15}$: Eu^{2+} , Mn^{2+} phosphors exhibit efficient blue and red emissions due to Eu^{2+} 4f-5d transition and Mn^{2+} 3d-3d transition, which matches well with the absorption of plant chlorophylls, and also could be excited by near ultraviolet LED chip. The emitting color could be readily tuned from blue through pink to red due to effective Eu^{2+} - Mn^{2+} energy transfer by changing Eu^{2+} / Mn^{2+} ratio. And the corresponding energy transfer mechanism is found to be dipole-dipole interaction. The thermal stability of $\text{Na}_2\text{Mg}_2\text{Si}_6\text{O}_{15}$: Eu^{2+} , Mn^{2+} is significantly higher than that of most reported Eu^{2+} , Mn^{2+} co-activated dual-emitting phosphors, due to thermally activated defect- Eu^{2+} - Mn^{2+} energy transfer process. Thus, it indicates that $\text{Na}_2\text{Mg}_2\text{Si}_6\text{O}_{15}$: Eu^{2+} , Mn^{2+} is of great potential as converted phosphors for plant growth application.

1. Introduction

In present days, LEDs are the main artificial light source for plant growth due to the advantages of high adjustability and energy saving, and have been widely used in indoor plant cultivation [1]. The photosynthetic action spectrum (PAS) shows the characteristic absorption bands of plants chlorophylls in the range of 600–700 nm red light and that of 400–500 nm blue light. To be exact, blue light (400–500 nm), red light (620–690 nm) and far-red light (700–740 nm) play vital roles in reactions of photosynthesis, phototropism, and photomorphogenesis [2, 3]. Thus, tuning artificial lighting source to have a perfect match with PAS is of great importance in indoor plant growth process. The phosphor-converted LEDs sources covering the whole PAS shows a great potential for plant illumination purpose, since multi-chips LEDs suffer from spectrum mismatch with PAS due to the narrow emissions of LED chip, as well as severe thermal quenching under high-power drive [4]. For the converted phosphors used in plant growth lighting sources, it must have the broadband emissions which could perfectly match the

PAS, with good thermal stability for high-power drive and long-term usage. Single-phased multicolor-emitting phosphor is an ideal choice for satisfy above mentioned requirements. Using energy transfer strategy, efficient phosphors with well-matched multiple-emission bands have been designed and synthesized like $\text{Ba}_3\text{CaK}(\text{PO}_4)_3$: Eu^{2+} [5] and $\text{Ca}_{19}\text{Zn}_2(\text{PO}_4)_{14}$: Eu^{2+} , Mn^{2+} [6]. However, most of the reported converted phosphors show severe emission quenching at high temperature [7]. Therefore, it is essential to develop novel dual-emitting phosphor with thermally stable luminescence.

Alkaline silicates have special merits as phosphor host, such as high rigidity and cuboidal alkaline sites, which could result in the efficient broadband emission and high thermal stability. Promising luminescent properties of Eu^{2+} -activated alkali silicate phosphors such as $\text{RbNa}_3\text{Li}(\text{Li}_3\text{SiO}_4)_4$: Eu^{2+} [8], $\text{RbLi}(\text{Li}_3\text{SiO}_4)_2$: Eu^{2+} [9] and $\text{Li}_3\text{NaSiO}_4$: Eu^{2+} [10] have been reported. In this study, a tuhualite-structure alkali silicate, $\text{Na}_2\text{Mg}_2\text{Si}_6\text{O}_{15}$ [11], is chosen as phosphor host. The thermal stable blue emission in Eu^{2+} -activated $\text{Na}_2\text{Mg}_2\text{Si}_6\text{O}_{15}$ has been reported by Toda et al. [12], but the luminescence of Eu^{2+} , Mn^{2+} co-doped $\text{Na}_2\text{Mg}_2\text{Si}_6\text{O}_{15}$

* Corresponding author.

** Corresponding author. Department of Pharmacy, Shenzhen Hospital, Southern Medical University, Shenzhen, 518101, China.

*** Corresponding author.

E-mail addresses: yixiao@163.com (X. Yang), yuzq@smu.edu.cn (Z. Yu), mpcc1@qq.com (X. Zhang).

was not reported yet. Here, Eu^{2+} , Mn^{2+} co-doped $\text{Na}_2\text{Mg}_2\text{Si}_6\text{O}_{15}$ phosphors could exhibit efficient blue and red emission at 430 and 630 nm due to Eu^{2+} 4f-5d transition and Mn^{2+} 3d-3d transition, which exactly satisfies photosynthetic action spectrum. More importantly, using the strategy of defect- Eu^{2+} - Mn^{2+} energy transfer, the phosphor shows promising emission thermal stability, i.e. blue and red emission keeps about 71.3% and 82.6% of original intensity at 200 °C. All result indicates that the prepared dual-emitting $\text{Na}_2\text{Mg}_2\text{Si}_6\text{O}_{15}$: Eu^{2+} , Mn^{2+} have potential application value as converted phosphor in indoor plant-growth lighting.

2. Experimental detail

2.1. Sample synthesis

Series of solid-state solutions with the formula of $\text{Na}_{2-x}\text{Mg}_{2-y}\text{Si}_6\text{O}_{15}$: $x\text{Eu}^{2+}$, $y\text{Mn}^{2+}$ ($x = 0.02$, $y = 0\text{--}0.80$) were prepared by solid-state reaction method. The Na_2CO_3 , $4\text{MgCO}_3\cdot\text{Mg(OH)}_2\cdot 6\text{H}_2\text{O}$, SiO_2 , MnCO_3 and Eu_2O_3 powders with high purity were employed as the raw materials. The stoichiometric starting materials were weighed and mixed thoroughly in an agate mortar. Then these mixed powders were kept in a crucible and sintered at the temperature of 1100 °C for 5 h in the H_2 reducing atmosphere. Finally, the final products were obtained when the furnace cooled down to room temperature naturally.

2.2. Characterization

The phase structures of the $\text{Na}_{2-x}\text{Mg}_{2-y}\text{Si}_6\text{O}_{15}$: $x\text{Eu}^{2+}$, $y\text{Mn}^{2+}$ were characterized using a powder X-ray diffractometer (XRD) (Bruker D8 ADVANCE) with $\text{Cu K}\alpha$ irradiation ($\lambda = 1.5406$ nm) operating at 40 kV and 40 mA. The scanning rate was fixed at 5°/min to record in the 2θ range from 10° to 80°. Photoluminescence excitation (PLE) spectra, photoluminescence (PL) spectra and fluorescence lifetime were determined using a FLS 980 Fluorescence Spectrophotometer (Edinburgh). The surrounding temperature of the products in the range of 293–473 K was adjusted by the temperature-controlled stage (OptistatDN). The duration of thermal treatment for PL spectrum at each temperature point is about 5 min. For example, after temperature reaches at 473 K, it takes

3 min to stabilize the temperature in range of 473 ± 0.1 K, then 2 min to finish the corresponding PL measurement. The decay curves were measured by using the same spectrofluorometer equipped with a 320 nm laser and a pulsed xenon lamp.

3. Results and discussion

3.1. Phase identification & structure characterization

XRD patterns of the typical samples of $\text{Na}_2\text{Mg}_2\text{Si}_6\text{O}_{15}$ host, $\text{Na}_2\text{Mg}_2\text{Si}_6\text{O}_{15}$: 0.02Eu²⁺, $\text{Na}_2\text{Mg}_2\text{Si}_6\text{O}_{15}$: 0.20Mn²⁺ and $\text{Na}_2\text{Mg}_2\text{Si}_6\text{O}_{15}$: 0.02Eu²⁺, 0.60Mn²⁺ are displayed in Fig. 1a. The synthesized samples were indexed to the standard data of $\text{Na}_2\text{Mg}_2\text{Si}_6\text{O}_{15}$ (JCPDS 70-1506) without secondary phase and impurities, indicating that Eu²⁺/Mn²⁺ ions have a high solubility limit in the $\text{Na}_2\text{Mg}_2\text{Si}_6\text{O}_{15}$. The charge balance and effective ionic radius results of the cations showed that Eu²⁺ (coordination number (CN) = 6 for 1.17 Å) and Mn²⁺ (CN = 4 and 6 for 0.66 and 0.83 Å) preferentially substitute the sites of Na⁺ (CN = 6 for 1.02 Å) and Mg²⁺ (CN = 4 and 6 for 0.57 and 0.72 Å) in the $\text{Na}_2\text{Mg}_2\text{Si}_6\text{O}_{15}$ host. The enlarged XRD profiles (Fig. 1b) show that the diffraction peaks shift to lower angles as the content of Mn²⁺ increases in the $\text{Na}_2\text{Mg}_2\text{Si}_6\text{O}_{15}$ host. In a similar crystal structure, replacing smaller cations with larger cations expands the crystal cells. Based on the Bragg's equation ($2d \times \sin \theta = n\lambda$), the expansion of the cell volume decreases the 2θ value, which suggests that the lattice expands as the smaller Mg²⁺ ion was replaced by the larger Mn²⁺ ion in $\text{Na}_2\text{Mg}_2\text{Si}_6\text{O}_{15}$ host. In order to figure out the cell parameters variation, Rietveld refinement was performed by JADE 6.0 software, and the results are displayed in Fig. 1c. It is found that both the edge length a , b , c and cell volume V increase generally, which is in good agreement with the fact that the effective ion radius of Mn²⁺ is larger than that of Mg²⁺.

The crystal structure of the $\text{Na}_2\text{Mg}_2\text{Si}_6\text{O}_{15}$ unit cell along with the coordination environment of the Na⁺ and Mg²⁺ ions is demonstrated in Fig. 2. The $\text{Na}_2\text{Mg}_2\text{Si}_6\text{O}_{15}$ system was composed of tetragonal Si-O and formed a 3-dimensional (3D) network structure. The Na⁺ ions possessed two different sites which were marked as Na1 and Na2 with coordination number of 7 and 6, respectively. Besides, the Mg1 ions were surrounded by 4 oxygen ions with Mg1-O bond length of 1.965 Å, and the

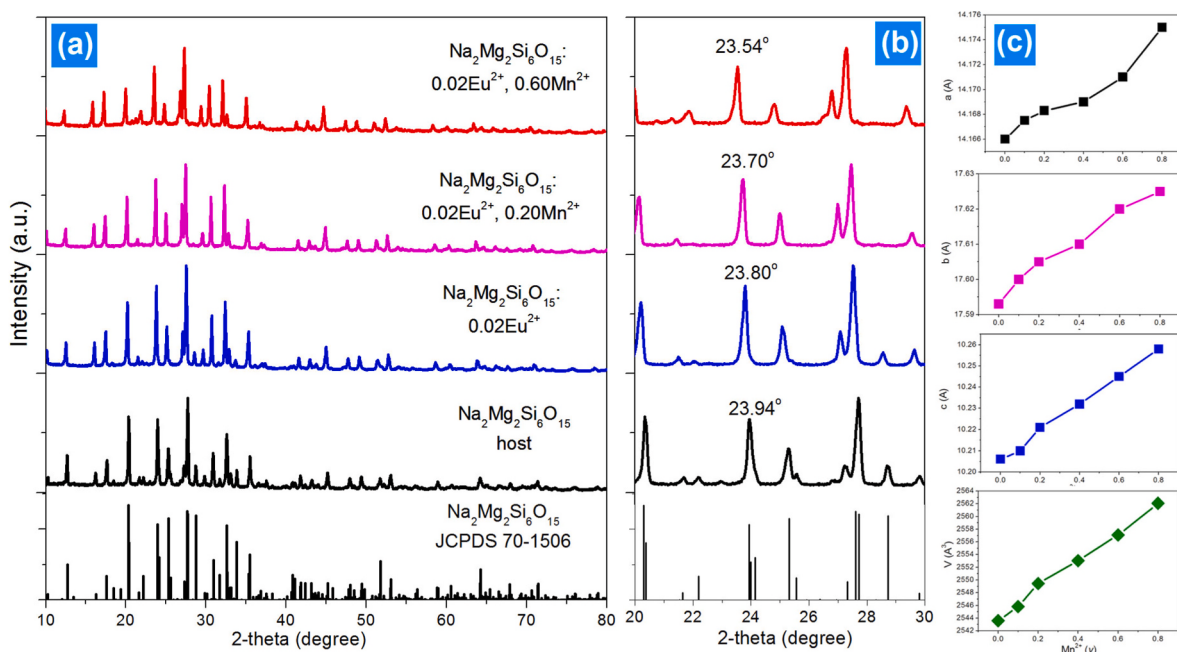


Fig. 1. (a) The typical XRD patterns of as-prepared samples together with the standard data (ICSD 2850), (b) the enlargement in the range of 20–30, (c) variation of lattice parameters.

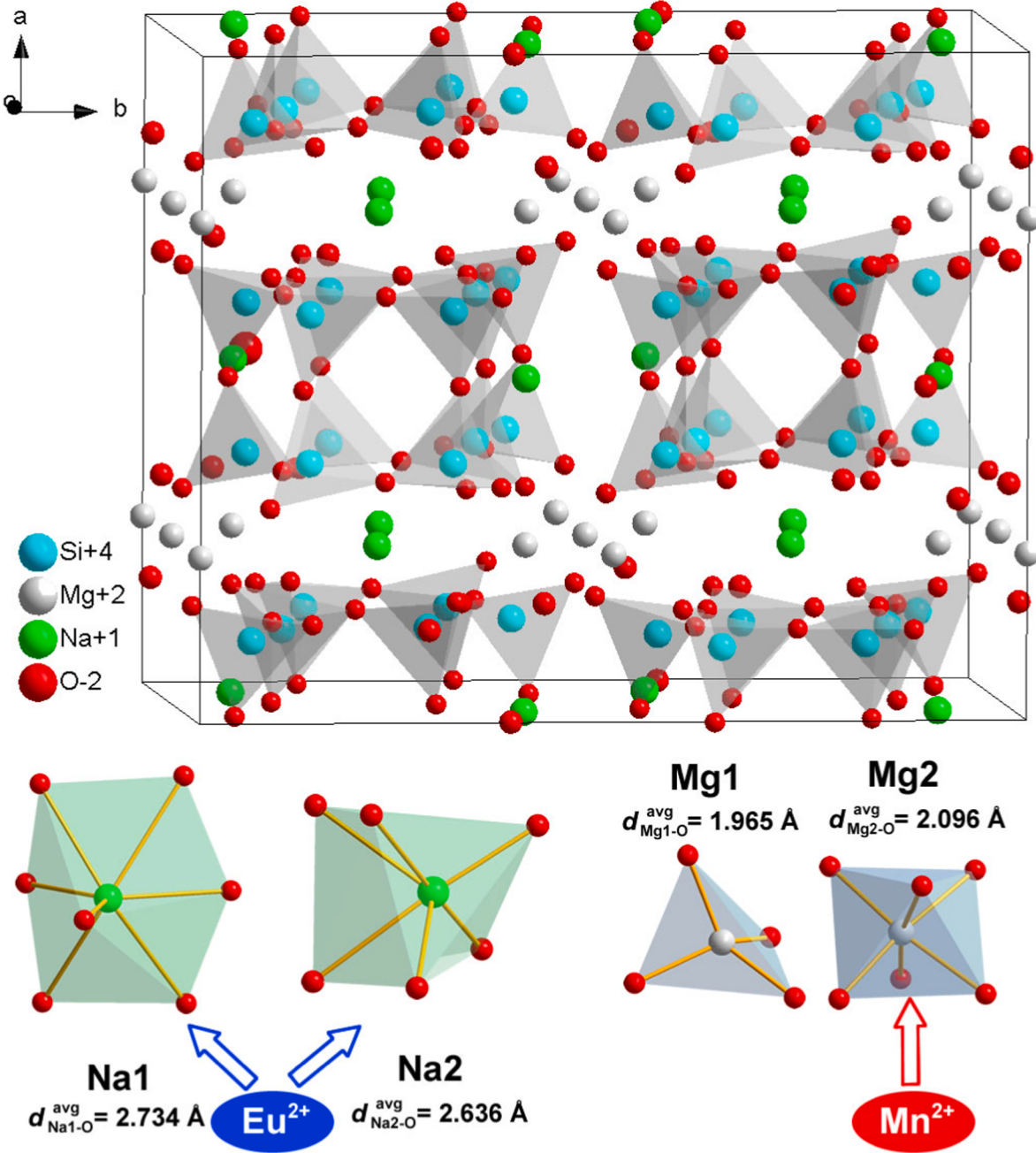


Fig. 2. Crystal structure of the $\text{Na}_2\text{Mg}_2\text{Si}_6\text{O}_{15}$ unit cell along with coordination environment of the Na^+ and Mg^{2+} ions.

Mg^{2+} ions were coordinated with 6 oxygen ions with $\text{Mg}^{2+}\text{-O}$ bond length of 2.096 Å. Considering the similar valency and close radii between the Na^+ and Eu^{2+} ions, the Eu^{2+} ions could randomly occupy the positions of Na^+ ions in the $\text{Na}_2\text{Mg}_2\text{Si}_6\text{O}_{15}$ host lattices. Due to the valence difference between Na^+ and Eu^{2+} , negatively-charged Na vacancies (V'_{Na}) could be introduced and acted as defect level during the doping process as:



The relationship between various Eu^{2+} -emitting centers and the corresponding luminescent property in the Eu^{2+} -doped $\text{Na}_2\text{Mg}_2\text{Si}_6\text{O}_{15}$ system has been investigated by Toda et al. [12]. Meanwhile, Mn^{2+} dopant could occupy either 4-coordinated $\text{Mg}1$ or 6-coordinated $\text{Mg}2$ site, depending on the similarity of both valence and ionic radius. The exact Mn^{2+} occupied site could be identified by its emission property, as discussed in Section 3.2.

3.2. Luminescence properties & energy transfer

The excitation spectrum of Eu^{2+} single-doped $\text{Na}_2\text{Mg}_2\text{Si}_6\text{O}_{15}$ phosphor, which was monitored at 430 nm, are demonstrated in Fig. 3a. The excitation spectra exhibited broad band in the range of 250–400 nm arising from the $4f^7$ to $4f^65d^1$ states of the Eu^{2+} ions. The corresponding emission spectrum, which was excited at 365 nm, showed one asymmetric emission band at 430 nm triggered by the $\text{Eu}^{2+} 4f^65d^1 \rightarrow 4f^7$ transition. In order to understand the occupation properties of Eu^{2+} ions, Toda et al. have employed the Gaussian fitting algorithm to separating the emission band as two components at 430 and 460 nm, which was assigned to Eu^{2+} located in $\text{Na}1$ and $\text{Na}2$ site, respectively [12].

Furthermore, the emission band of $\text{Na}_2\text{Mg}_2\text{Si}_6\text{O}_{15}$: Eu^{2+} is asymmetric shape because Eu^{2+} occupies two sites, $\text{Na}1\text{O}_7$ and $\text{Na}2\text{O}_6$. Thus, Gaussian deconvolution of the emission spectrum is applied, and two components at 430 and 460 nm are separated (Fig. 3a). It is well-known

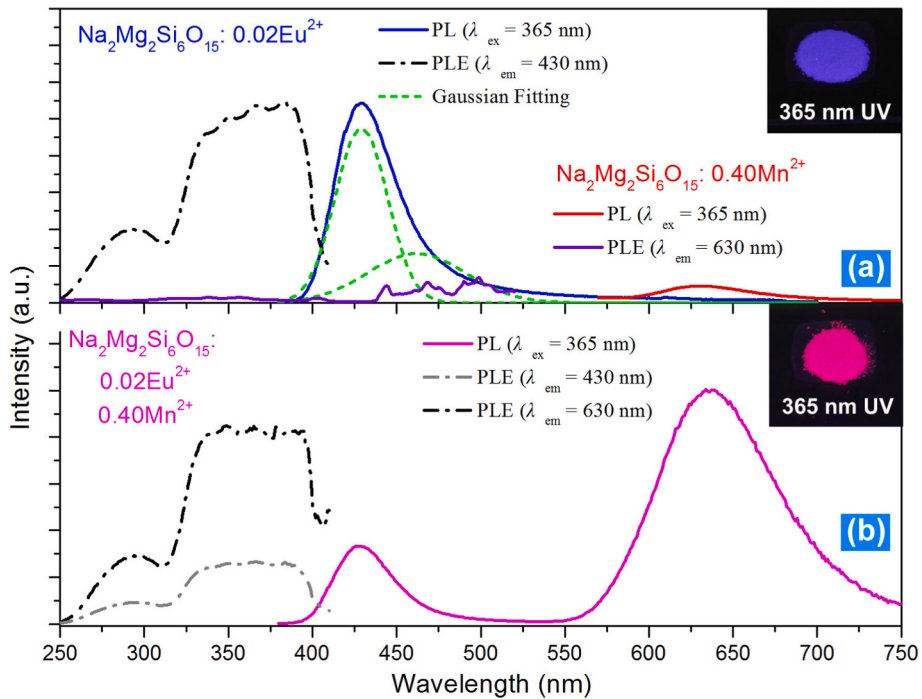


Fig. 3. Excitation and emission spectra of Na₂Mg₂Si₆O₁₅: Eu²⁺/Mn²⁺ (a) and Na₂Mg₂Si₆O₁₅: 0.02Eu²⁺, 0.40Mn²⁺ (b), inset are the corresponding sample pictures under 365 nm UV light.

that the emission energy of Eu²⁺ ions in different crystal environments could be roughly evaluated:

$$E = Q \left[1 - \left(\frac{V}{4} \right)^{\frac{1}{n}} 10^{-\frac{nE_a}{30}} \right] \quad (2)$$

E was d-band edge of Eu²⁺ ions (cm⁻¹) in energy, Q was the energy position for the lower d-band edge of free Eu²⁺ ions (34,000 cm⁻¹), $V = 2$, which referred to the valence of Eu²⁺, n was the coordinated number around Eu²⁺, r was average bond distance of sites, and E_a was the electron affinity of the anion group (eV). The value of E is directly proportionate to $n \times r$. Since the average bond length of Na₂O₆ (2.636 Å) is smaller than that of NaO₇ (2.734 Å), 430 and 460 nm sub-peak was assigned to Eu²⁺ located in Na1 and Na2 site, respectively.

The emission intensity of Mn²⁺ solo-doped phosphor is very weak due to the forbidden nature of Mn²⁺ ${}^4T_1 \rightarrow {}^6A_1$ transition. The PL spectrum of Mn²⁺ single-doped Na₂Mg₂Si₆O₁₅ exhibits one band at 630 nm, indicating that Mn²⁺ ions prefer to substitute octahedral coordination sites. The corresponding excitation spectrum presents several weak absorption bands at 423, 478, and 562 nm, which are due to the transitions from ${}^6A_1 \rightarrow {}^4A_{1g}$ (4G)), ${}^4T_{2g}$ (4G), and ${}^4T_{1g}$ (4G) levels of Mn²⁺, respectively. A significant spectra overlap could be observed between Eu²⁺ emission band and the Mn²⁺ excitation transitions, indicating that an efficient energy transfer from Eu²⁺ to Mn²⁺ is expected. Normally, the Mn²⁺ emitting color is strongly dependent on the coordination environment of Mn²⁺ in the host lattice [13]. Tetrahedrally coordinated Mn²⁺ usually gives a green emission, while the octahedrally coordinated Mn²⁺ gives an orange to deep red emission [14]. Since there are two available Mg²⁺ sites for Mn²⁺ occupation, i.e. tetrahedral Mg1 and octahedral Mg2. As a consequence, red emission is eventually attributed to ${}^4T_1 \rightarrow {}^6A_1$ transition of Mn²⁺ incorporated in Mg2 site of the Na₂Mg₂Si₆O₁₅ host lattice.

The excitation and emission spectra of representative Na₂Mg₂Si₆O₁₅: 0.02Eu²⁺, 0.40Mn²⁺ sample were illustrated in Fig. 3b. The emission spectrum of Eu²⁺, Mn²⁺ co-doped Na₂Mg₂Si₆O₁₅ phosphor had two distinct broad emission bands with peaks at 430 and 630 nm, respectively. The blue emission was originated from the Eu²⁺ ions in

Na₂Mg₂Si₆O₁₅ host, and the wide emission band in red region was ascribed to ${}^4T_1 \rightarrow {}^6A_1$ transition of the Mn²⁺ ions. The excitation spectra of the Na₂Mg₂Si₆O₁₅: 0.02Eu²⁺, 0.40Mn²⁺ sample by monitoring 430 and 630 nm emission were consisted of similar broad absorption bands covering the whole UV region with different intensity, suggesting that energy transfer is occurring from sensitizer Eu²⁺ to activator Mn²⁺, and Eu²⁺, Mn²⁺ co-doped Na₂Mg₂Si₆O₁₅ could efficiently convert UV light to double emission. The suitable emitting spectrum of Na₂Mg₂Si₆O₁₅: 0.02Eu²⁺, 0.40Mn²⁺ phosphor covered all the PAS of plants chlorophylls indicates its potential application in plant illumination combining with near-UV LED chips.

The Mn²⁺ concentration-dependent emission spectra of Na₂-0.02Mg₂-ySi₆O₁₅: 0.02Eu²⁺, yMn²⁺ phosphors have been measured and demonstrated in Fig. 4a. As displayed, all of the detected luminescent profiles, which consisted of the emission peaks of both Eu²⁺ and Mn²⁺, were similar; despite the emission intensities were sensitive to the doping concentration. The blue emission of Eu²⁺ showed a monotonous decrease as the Mn²⁺ content increased. The red emission of Mn²⁺ showed an initial increase reaching a maximum at $y = 0.6$, followed by a continuous decrease due to concentration quenching. The quantum efficiency of optimal sample Na₂Mg₂Si₆O₁₅: 0.02Eu²⁺, 0.60Mn²⁺ is 51%. With an increase in the Mn²⁺ doping content, the gradual decrease in Eu²⁺ emission intensity verifies the occurrence of Eu²⁺-Mn²⁺ energy transfer process. Based on the variation of sensitizer Eu²⁺ emission intensity, the energy transfer efficiency (η_{ET}) can be calculated using the following equation [15]:

$$\eta_{ET} = 1 - I/I_0 \quad (3)$$

where I_0 and I are the Eu²⁺ emission intensity in the Eu²⁺ single-doped and Eu²⁺, Mn²⁺ co-doped samples, respectively. As evidenced in Fig. 4a inset, the η_{ET} for the $y = 0.80$ sample reached as high as 98.8 %. This efficient energy transfer will be beneficial to realize the color-tunable luminescence from blue to red in the Na₂Mg₂Si₆O₁₅: Eu²⁺, Mn²⁺ samples under UV light excitation (Fig. 4b).

As observed in Fig. 4a, a continuous red-shift is observed on the peak wavelength of Mn²⁺ along with increasing Mn²⁺ concentration. There

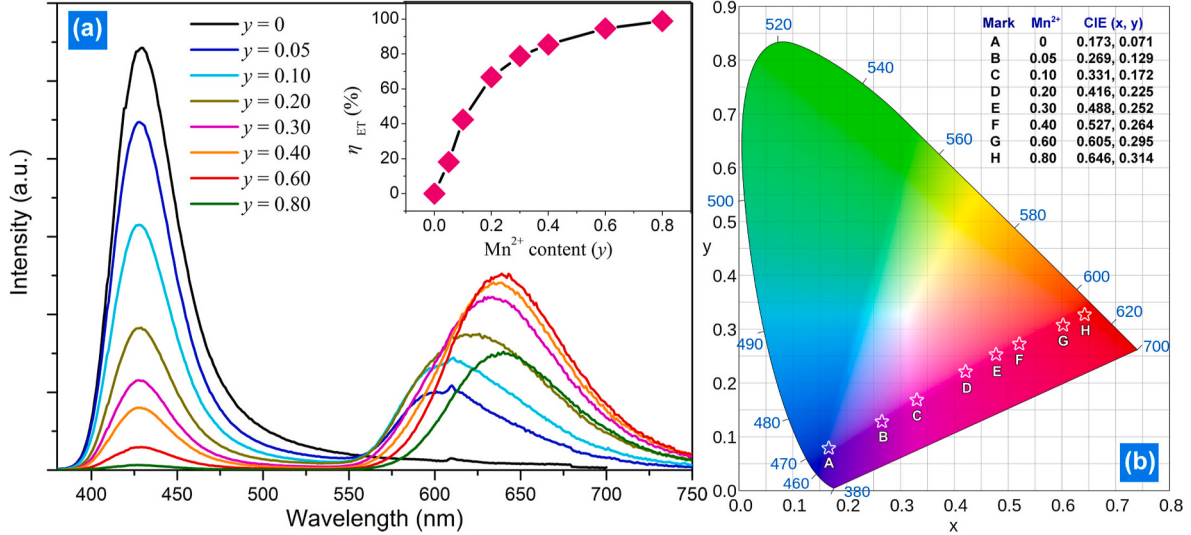


Fig. 4. The emission spectra of $\text{Na}_{2-x}\text{Mg}_{2-y}\text{Si}_6\text{O}_{15} : x\text{Eu}^{2+}, y\text{Mn}^{2+}$ ($x = 0.02, y = 0-0.80$) upon 365 nm excitation (a), and the corresponding CIE diagram (b).

are two aspects can be explained this phenomenon. On the one hand, since the ion radius of Mn²⁺ is larger than Mg²⁺, the Mn-O distances would shorten with consistent Mn²⁺ replacement of Mg²⁺, which result in the stronger crystal field and emission red shift. On the other hand, the probability of the energy transfer between the Mn²⁺ ions is increased via decreasing the average distance between Mn²⁺ ion. The nonradiative energy transfer would lead to the excited 5d electron transfer to a relatively lower energy level. Thus, a redshift emission is observed with increasing Mn²⁺ concentration [16]. Fig. 5b shows the CIE coordinates variation of $\text{Na}_{2-0.02}\text{Mg}_{2-y}\text{Si}_6\text{O}_{15} : 0.02\text{Eu}^{2+}, y\text{Mn}^{2+}$ phosphors.

It is well-known that the main mechanism of energy transfer can be include in two types: exchange interaction or electric multipolar interaction. To have a further investigation of the process of energy transfer between the Mn²⁺ ions, the critical distance for energy transfer can be obtained by Ref. [17]:

$$R_c \approx 2 \left(\frac{3V}{4\pi x_c N} \right)^{1/3} \quad (4)$$

in which V means the unit cell volume (2542.7 \AA^3), x_c represents the concentration of Mn²⁺ ion where the quenching occurs (0.60) and N is the number of the Mg²⁺ ion in per unit cell (16). Hence, the value of R_c is calculated to about 7.967 \AA . Since the typical critical distance of the exchange interaction is 5 \AA or less, therefore, the electric multipolar interactions are dominant in the intra-Mn²⁺ energy transfer.

To further discuss the energy transfer from Eu²⁺ to Mn²⁺ ions, the fluorescent decay curves of Eu²⁺ in different Mn²⁺ doping contents, which are monitored at 430 nm and excited at 320 nm laser, were depicted in Fig. 5a. All decay curves can be well fitted to a bi-exponential decay model:

$$I(t) = A_1 \exp\left(-\frac{t}{\tau_1}\right) + A_2 \exp\left(-\frac{t}{\tau_2}\right) \quad (5)$$

where I is the luminescence intensity; A_1 and A_2 are constants; t is the time; and τ_1 and τ_2 are the lifetimes for the exponential components. And the effective decay lifetime values were calculated by:

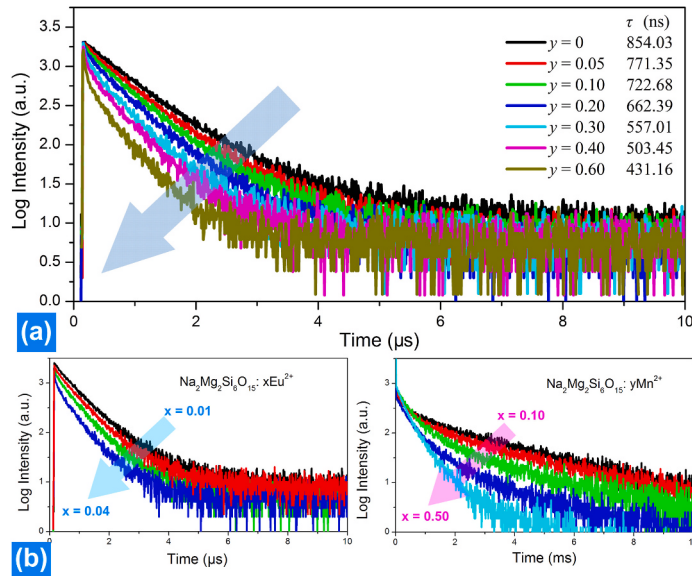


Fig. 5. Decay lifetime curves monitored at 430 nm Eu²⁺ emission in $\text{Na}_2\text{Mg}_2\text{Si}_6\text{O}_{15} : \text{Eu}^{2+}, \text{Mn}^{2+}$ (a), Eu²⁺ and Mn²⁺ decay lifetime data in Eu²⁺/Mn²⁺-singly doped $\text{Na}_2\text{Mg}_2\text{Si}_6\text{O}_{15}$ (b) and schematic diagram of energy transfer (c).

$$\tau = \frac{\int_0^\infty I(t) dt}{\int_0^\infty I(t)^2 dt} \quad (6)$$

The effective decay lifetimes were 854, 771, 722, 662, 557, 503 and 431 ns for the samples $\text{Na}_2\text{Mg}_{2-y}\text{Si}_6\text{O}_{15}$: 0.02Eu²⁺, yMn²⁺ ($y = 0, 0.05, 0.10, 0.20, 0.30, 0.40$ and 0.60), respectively. The decay lifetime of Eu²⁺ monotonously decreased as the Mn²⁺ content increased, and this firmly demonstrated the energy transfer from Eu²⁺ to Mn²⁺. Both Eu²⁺ and Mn²⁺ decay lifetime data in Eu²⁺/Mn²⁺-singly doped Na₂Mg₂Si₆O₁₅ are shown in Fig. 5b, which make possible to exactly clarify the effects of co-doping Eu²⁺/Mn²⁺ in Na₂Mg₂Si₆O₁₅. The proposed diagram of the energy transfer process from Eu²⁺ to Mn²⁺ in Na₂Mg₂Si₆O₁₅ phosphor is illustrated in Fig. 5c. From this diagram, the energy transfer behavior between Eu²⁺ and Mn²⁺ ions can be attributed to the similar value of energy level between the excited 5d state of Eu²⁺ and the ⁴T₁ levels of Mn²⁺ ions.

To identify the exact Eu²⁺-Mn²⁺ energy transfer mechanism in Na₂Mg₂Si₆O₁₅, Reisfeld's approximation was applied, i.e. the relation between the sensitizer Eu²⁺ emission intensity and Mn²⁺ concentration can be expressed as [18]:

$$\frac{I_0}{I} \propto (C_{\text{Mn}})^{s/3} \quad (7)$$

while the values of s can be 6, 8 and 10 corresponding to the dipole-

dipole, dipole-quadrupole and quadrupole-quadrupole interactions, respectively. The exponential fitting model was used to analyze the raw data, as shown in Fig. 6. A linear fitting results was found when the value of s was 6, implying that the electric dipole-dipole interaction was responsible for Eu²⁺-Mn²⁺ energy transfer in Na₂Mg₂Si₆O₁₅.

3.3. Emission thermal stability

It is quite important for phosphor materials to measure the thermal stability at high temperature because the temperature in most of luminescent devices rises when they are driven. Since the high power or laser lighting gradually becomes the main streams with the development of lighting industry, and the thermally stable luminescence is badly needed in near future [19,20].

Upon the excitation at 365 nm, the temperature-dependent emission spectra of the Na₂Mg₂Si₆O₁₅: 0.02Eu²⁺ phosphors were measured in the range of 20–200 °C, as displayed in Fig. 7a. The total integrated emission intensity decreased continuously with the temperature, which was triggered by the thermal quenching effect, and kept at around 68.6% of its starting value at 20 °C as the temperature heating up to 200 °C. It is quite amazing to find out that the emission thermal stability is enhanced by Eu²⁺, Mn²⁺ co-doped. As seen in Fig. 7b, in case of Na₂Mg₂Si₆O₁₅: 0.02Eu²⁺, 0.20Mn²⁺ sample, the relative intensity of Eu²⁺ blue emission at 200 °C is 74.7% of original intensity at 20 °C, while that of Mn²⁺ red

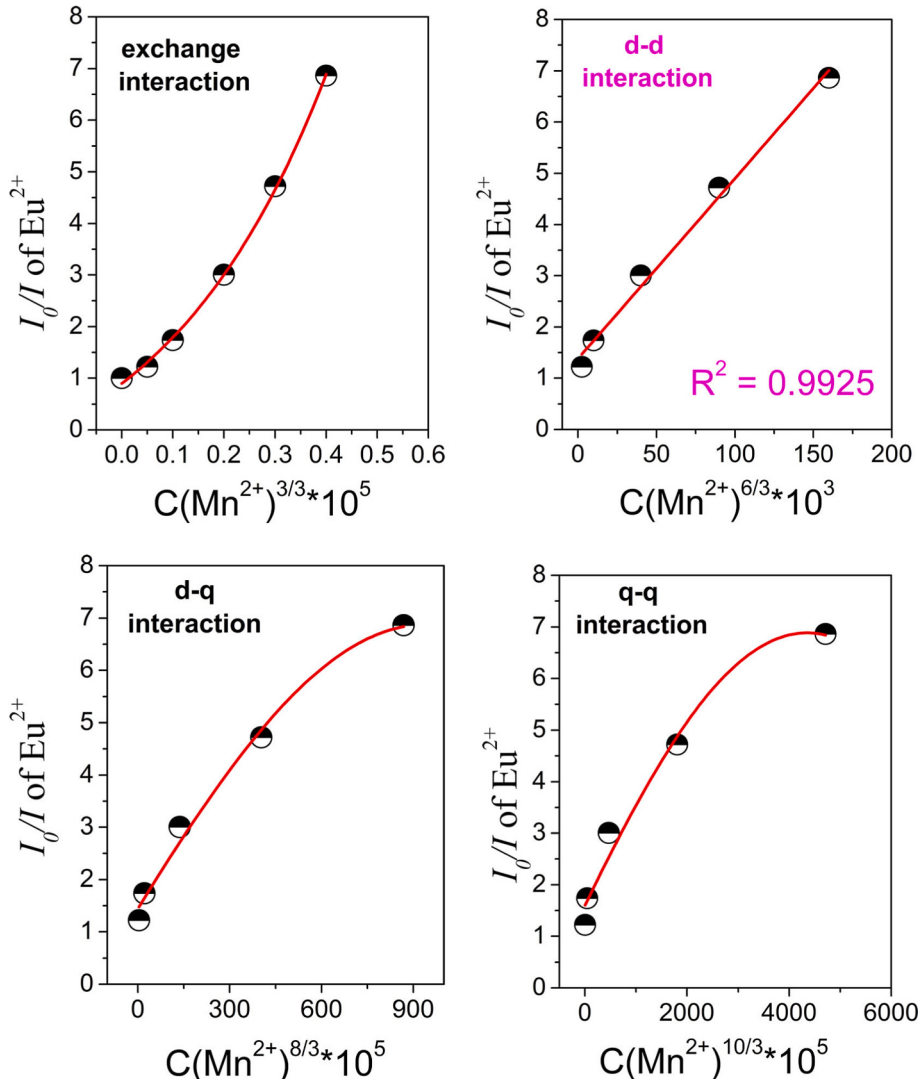


Fig. 6. Dependence of I_0/I of Eu²⁺ on $C_{\text{Mn}2+}^{s/3}$ ($s = 3, 6, 8$ and 10).

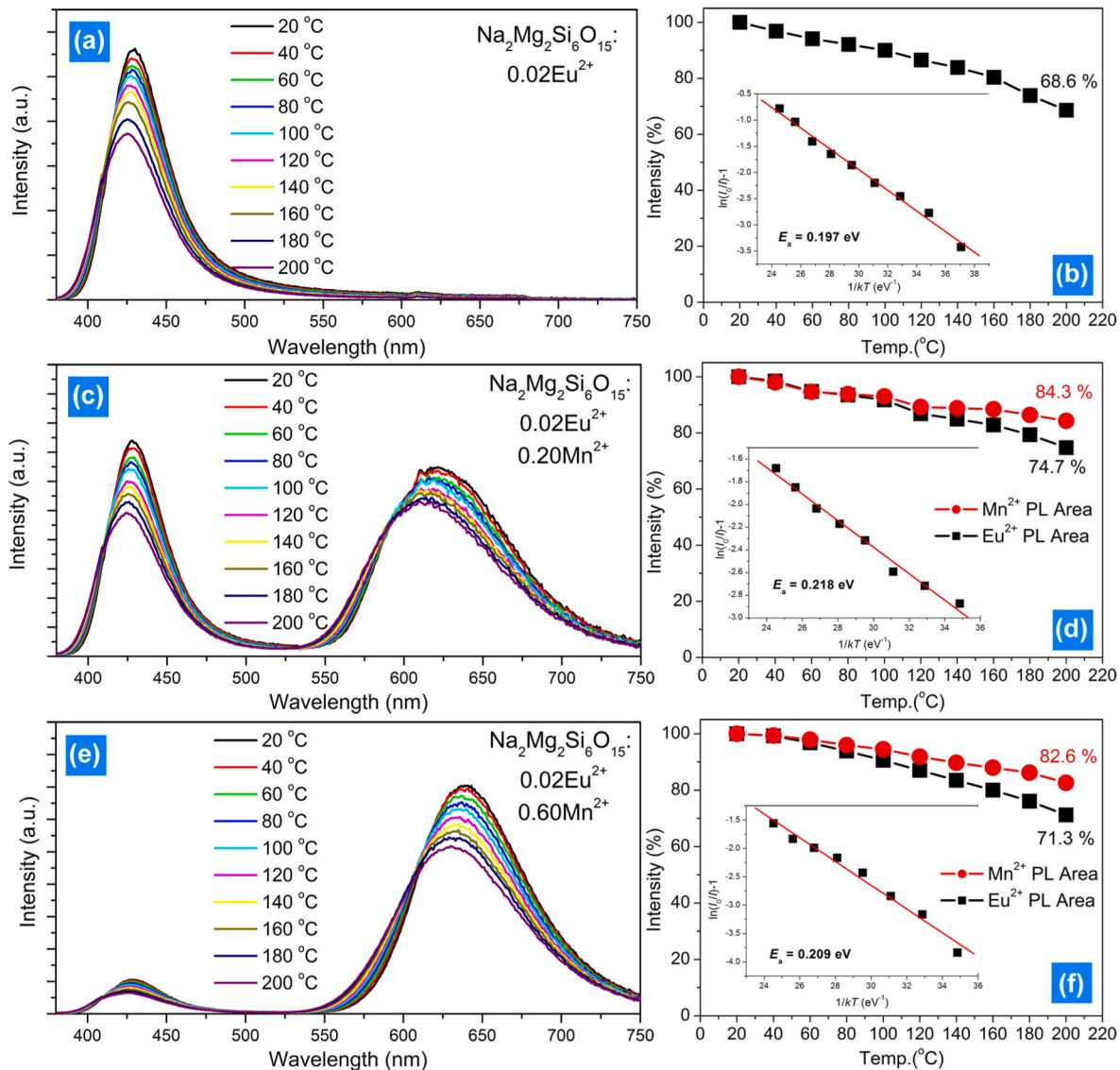


Fig. 7. Temperature-dependent PL spectra of $\text{Na}_2\text{Mg}_2\text{Si}_6\text{O}_{15} \cdot 0.02\text{Eu}^{2+}, y\text{Mn}^{2+}$ phosphors ($y = 0, 0.20$ and 0.60 for a, c, e), and corresponding normalized PL intensity as a function of temperature (b,d,f). Insets are the activated energy plotting.

emission showed a slight thermal quenching, i.e. 84.3% of original intensity at 200 °C. The Mn^{2+} heavily doping did not have significant negative effect on emission thermal stability. The blue and red emission intensity of optimized $\text{Na}_2\text{Mg}_2\text{Si}_6\text{O}_{15} \cdot 0.02\text{Eu}^{2+}, 0.60\text{Mn}^{2+}$ sample kept about 71.3% and 82.6% at 200 °C. In addition, a blue shift of the Mn^{2+} emission from red occurred at high temperatures possibly as a result of thermally activated phonon-assisted excitation from lower excited states to higher ones in Mn^{2+} . The result indicates that the thermal stability of $\text{Na}_2\text{Mg}_2\text{Si}_6\text{O}_{15} \cdot \text{Eu}^{2+}, \text{Mn}^{2+}$ is considerably higher than that of most reported $\text{Eu}^{2+}, \text{Mn}^{2+}$ co-activated dual-emitting phosphors, such as $\text{K}_2\text{BaCa}(\text{PO}_4)_2 \cdot \text{Eu}^{2+}, \text{Mn}^{2+}$ [21] and $(\text{Ba}_{0.9}\text{Sr}_{0.1})_9\text{Lu}_2\text{Si}_6\text{O}_{24} \cdot \text{Eu}^{2+}, \text{Mn}^{2+}$ [22]. Therefore, $\text{Na}_2\text{Mg}_2\text{Si}_6\text{O}_{15} \cdot \text{Eu}^{2+}, \text{Mn}^{2+}$ phosphor can be useful under the high temperature environment such as high-power driving luminescent device. It is well known that a phosphor of large activation energy promises good stability at high temperatures. The activation energy (E_a) was used to evaluate the emission thermal stability of phosphor and could be determined by Arrhenius equation. The E_a value was derived to be 0.197, 0.218 and 0.209 eV for $\text{Na}_2\text{Mg}_2\text{Si}_6\text{O}_{15} \cdot 0.02\text{Eu}^{2+}$, $\text{Na}_2\text{Mg}_2\text{Si}_6\text{O}_{15} \cdot 0.02\text{Eu}^{2+}$, 0.20Mn^{2+} and $\text{Na}_2\text{Mg}_2\text{Si}_6\text{O}_{15} \cdot 0.02\text{Eu}^{2+}, 0.60\text{Mn}^{2+}$, respectively.

According to previous study, It is revealed that the vacancies that

generate when Eu^{2+} was doped into alkaline sites could act as an electron trap, and assist the thermal stability at high temperature by release the electron from the trap levels to the emission level of Eu^{2+} . Using the strategy of energy transfer from defect levels to Eu^{2+} 5d-band, high thermally stable phosphor $\text{K}_2\text{BaCa}(\text{PO}_4)_2 \cdot \text{Eu}^{2+}$ [23], $\text{Na}_3\text{Sc}_2(\text{PO}_4)_3 \cdot \text{Eu}^{2+}$ [24], $\text{K}_{x}\text{Cs}_{1-x}\text{AlSi}_2\text{O}_6 \cdot \text{Eu}^{2+}$ [25] exhibit zero-TQ phenomenon. Thus, this strategy should be used as an effective method to enhance thermal stability of phosphors. In present case, We believe that the thermally activated defect- Eu^{2+} - Mn^{2+} energy transfer is the main reason for the greatly enhanced thermal stability (Fig. 5b). Similar case has been found in $\text{BaMgP}_2\text{O}_7 \cdot \text{Eu}^{2+}, \text{Mn}^{2+}$, which realized zero-thermal quenching of Mn^{2+} red luminescence [26,27]. The generated defect levels are considered to play a crucial role in this processes. Under UV excitation, the traps will be filled with electrons and the holes are generated at valence band at the same time. Then the energy of electron-hole pairs can transfer to the Eu^{2+} 5d-band at high temperature, and transfer to Mn^{2+} 3d level with sensitized red transition. There is a great probability for more excited electrons overcoming the energy barrier to transfer the energy to Mn^{2+} excited levels in the energy transfer process from Eu^{2+} to Mn^{2+} resulting from stronger electron-phonon coupling with increasing temperature, which

effectively counter-measure non-radiative relaxation process. Consequently, the Mn^{2+} emission intensity of $Na_2Mg_2Si_6O_{15}$: Eu^{2+} , Mn^{2+} show promising thermal stability at elevated temperature.

4. Conclusion

Eu^{2+} , Mn^{2+} co-activated $Na_2Mg_2Si_6O_{15}$ phosphors with dual blue and red emissions were synthesized by a solid-state reaction route in a reduction atmosphere. The investigation on the crystal structure and photoluminescent properties indicated that two different Na^+ sites were partially occupied by the Eu^{2+} ions, while Mn^{2+} was selectively located in 6-coordinated Mg^2 site.

It is found that the emission spectrum of $Na_2Mg_2Si_6O_{15}$: Eu^{2+} , Mn^{2+} matched well the photosynthetic action spectrum (PAS) of plant chlorophylls. The optimal doping content for Mn^{2+} ions in the $Na_2Mg_2Si_6O_{15}$: Eu^{2+} , Mn^{2+} system was 0.60. The electric dipole-dipole interaction contributed to the involved Eu^{2+} , Mn^{2+} energy transfer process. The thermal stability performance was identified by using the temperature-dependent emission spectra. The blue and red emission intensity of optimized $Na_2Mg_2Si_6O_{15}$: 0.02 Eu^{2+} , 0.60 Mn^{2+} sample kept about 71.3% and 82.6% at 200 °C, which was significantly higher than that of most reported Eu^{2+} , Mn^{2+} co-activated dual-emitting phosphors. The corresponding reason could be thermally activated defect- Eu^{2+} - Mn^{2+} energy transfer, which acts as a countermeasure against non-radiative relaxation process. These results revealed that $Na_2Mg_2Si_6O_{15}$: Eu^{2+} , Mn^{2+} phosphors could be a novel promising luminescent material for plant growth LED based on the near-ultraviolet chip.

Credit author statement

Wanjun Gong: Writing – original draft. Jiabao Luo: XRD measurement. Weiyi Zhou: PL measurement. Jiaqi Fan: Temperature-dependent PL measurement. Senxiang Zeng: Sample preparation. Haowen Pan: XRD refinement. Zhenpeng Zhu: PL analysis. Xixiao Yang: Conceptualization. Zhiqiang Yu: Figure preparation. Xinguo Zhang: Writing- Reviewing and Editing.

Declaration of competing interest

The authors declare that they have no known competing financial interests or personal relationships that could have appeared to influence the work reported in this paper.

Acknowledgement

The work was supported by National Natural Science Foundation of China (No. 21601081) and Guangzhou Scientific planning program (No. 201804010260).

References

- [1] M. Xia, X. Wu, Z. Zhou, W. Wong, A novel $Na_3La(PO_4)_2/LaPO_4$: Eu blue-red dual-emitting phosphor with high thermal stability for plant growth lighting, *J. Mater. Chem. C.* 7 (2019) 2385–2393.
- [2] J. Chen, C. Yang, Y. Chen, J. He, Z.Q. Liu, J. Wang, J. Zhang, Local structure modulation induced highly efficient far-red luminescence of $La_{1-x}Lu_xAlO_3$: Mn^{4+} for plant cultivation, *Inorg. Chem.* 58 (2019) 8379–8387.
- [3] L. Shi, Y. Han, Z. Zhang, Z. Ji, D. Shi, X. Geng, H. Zhang, M. Li, Z. Zhang, Synthesis and photoluminescence properties of novel Ca_2LaSbO_6 : Mn^{4+} double perovskite phosphor for plant growth LEDs, *Ceram. Int.* 45 (2019) 4739–4746.
- [4] Z. Mao, J. Chen, J. Li, D. Wang, Dual-responsive Sr_2SiO_4 : Eu^{2+} – $Ba_3MgSi_2O_8$: Eu^{2+} , Mn^{2+} composite phosphor to human eyes and plant chlorophylls applications for general lighting and plant lighting, *Chem. Eng. J.* 284 (2016) 1003–1007.
- [5] J. Xiang, J. Zheng, Z. Zou, H. Suo, X. Zhao, X. Zhou, N. Zhang, M. Molokeev, C. Guo, Enhancement of red emission and site analysis in Eu^{2+} doped new-type structure $Ba_3CaK(PO_4)_3$ for plant growth white LEDs, *Chem. Eng. J.* 356 (2019) 236–244.
- [6] Z. Sun, Z. Zhu, J. Luo, Z. Guo, X. Zhang, Z. Wu, High-efficient and thermal-stable $Ca_19Zn_2(PO_4)_{14}$: Eu^{2+} , Mn^{2+} blue-red dual-emitting phosphor for plant cultivation LEDs, *J. Alloys Compd.* 811 (2019) 151956.
- [7] Z. Zhang, L. Shen, H. Zhang, L. Ding, G. Shao, X. Liang, W. Xiang, Novel red-emitting $CsPb_1-xTl_xI_3$ perovskite QDs@glasses with ambient stability for high efficiency white LEDs and plant growth LEDs, *Chem. Eng. J.* 378 (2019) 122125.
- [8] M. Zhao, Y. Zhou, M. Molokeev, Q. Zhang, Q. Liu, Z. Xia, Discovery of new narrow-band phosphors with the UCr_4C_4 -related type structure by alkali cation effect, *Adv. Opt. Mater.* 7 (2019) 1801631.
- [9] H. Liao, M. Zhao, Y. Zhou, M. Molokeev, Q. Liu, Q. Zhang, Z. Xia, Polyhedron transformation toward stable narrow-band green phosphors for wide-color-gamut liquid crystal display, *Adv. Funct. Mater.* 29 (2019) 1901988.
- [10] M. Iwaki, S. Kumagai, S. Konishi, A. Koizumi, T. Hasegawa, K. Uematsu, A. Itadani, K. Toda, M. Sato, Blue-yellow multicolor phosphor, Eu^{2+} -activated Li_3NaSiO_4 : excellent thermal stability and quenching mechanism, *J. Alloys Compd.* 776 (2019) 1016–1024.
- [11] M. Cradwick, H. Taylor, The crystal structure of $Na_2Mg_2Si_6O_{15}$, *Acta Crystallogr. B28* (1972) 3583.
- [12] M. Iwaki, K. Sugimoto, M. Watanabe, K. Uematsu, K. Toda, M. Sato, High thermal stable blue-emitting alkali silicate phosphor, Eu^{2+} -activated $Na_2Mg_2Si_6O_{15}$, *J. Ceram. Process. Res.* 20 (2019) 205–210.
- [13] L. Qin, C. Chen, J. Wang, S. Bi, Y. Huang, H. Seo, Luminescence properties of red-emitting Mn^{2+} -Activated $Na_2Mg_5Si_12O_{30}$ phosphors, *Mater. Res. Bull.* 118 (2019) 110949.
- [14] L. Wu, B. Wang, Y. Zhang, L. Li, R. Wang, H. Yi, Y. Kong, J. Xu, Structure and photoluminescence properties of a rare-earth free red-emitting Mn^{2+} -activated $KMgBO_3$, *Dalton Trans.* 43 (2014) 13845–13851.
- [15] X. Huang, H. Guo, L. Sun, T. Sakthivel, Y. Wu, A high-efficiency, broadband-excited cyan-emitting $Ba_3Lu_2B_6O_{15}$: Ce^{3+} , Tb^{3+} phosphor for near-UV-pumped white light-emitting diodes, *J. Alloys Compd.* 787 (2019) 865–871.
- [16] J. Chen, Y. Liu, L. Mei, Z. Wang, M. Fang, Z. Huang, Emission red shift and energy transfer behavior of color-tunable $KMg_4(PO_4)_3$: Eu^{2+} , Mn^{2+} phosphors, *J. Mater. Chem. C.* 3 (2015) 5516–5523.
- [17] L. Liang, L. Mei, L. Liu, C. Wang, L. Liao, Intense broad-band absorption and blue-emitting $Ca_9La(PO_4)_5(SiO_4)Cl_2$: Eu^{2+} phosphor under near-ultraviolet excitation, *J. Lumin.* 206 (2019) 154–157.
- [18] R. Cao, Y. Ran, X. Lv, L. Xu, H. Wan, Q. Hu, T. Chen, C. Cao, Tunable multicolor luminescent properties of $Ca_8ZnLa(PO_4)_7$: Ce^{3+} , Mn^{2+} phosphor via efficient energy transfer, *J. Lumin.* 214 (2019) 116549.
- [19] X. Zhang, Y. Huang, M. Gong, Dual-emitting Ce^{3+} , Tb^{3+} co-doped $LaOBr$ phosphor: luminescence, energy transfer and ratiometric temperature sensing, *Chem. Eng. J.* 307 (2017) 291–299.
- [20] X. Zhang, Z. Zhu, Z. Guo, Z. Sun, Y. Chen, A ratiometric optical thermometer with high sensitivity and superior signal discriminability based on $Na_3Sc_2P_3O_12$: Eu^{2+} , Mn^{2+} thermochromic phosphor, *Chem. Eng. J.* 356 (2019) 413–422.
- [21] X. Zhang, Z. Zhu, Z. Guo, Z. Sun, Z. Yang, T. Zhang, J. Zhang, Z. Wu, Z. Wang, Dopant preferential site occupation and high efficiency white emission in $K_2BaCa(PO_4)_2$: Eu^{2+} , Mn^{2+} phosphors for high quality white LED applications, *Inorg. Chem. Front.* 6 (2019) 1289–1298.
- [22] R. Dong, W. Liu, Y. Song, X. Zhang, Z. An, X. Zhou, K. Zheng, Y. Sheng, Z. Shi, H. Zou, A promising single-phase, color-tunable phosphor ($Ba_0.9Sr_0.1$) $9Lu_2Si_6O_{24}$: Eu^{2+} , Mn^{2+} for near-ultraviolet white-light-emitting diodes, *J. Lumin.* 214 (2019) 116585.
- [23] J. Qian, L. Ning, M. Molokeev, Y. Chuang, Q. Liu, Z. Xia, Eu^{2+} site preferences in the mixed cation $K_2BaCa(PO_4)_2$ and thermally stable luminescence, *J. Am. Chem. Soc.* 140 (2018) 9730–9736.
- [24] Y. Kim, P. Arunkumar, B. Kim, S. Unithrattil, E. Kim, S. Moon, J. Hyun, K. Kim, D. Lee, J. Lee, W. Im, A zero-thermal-quenching phosphor, *Nat. Mater.* 16 (2017) 543–550.
- [25] M. Zhang, Z. Xia, Q. Liu, Thermally stable phosphors $K_xCs_1-xAlSi_2O_6$: Eu^{2+} and tuning of photoluminescence, *J. Mater. Chem. C.* 5 (2017) 7489–7494.
- [26] R. Shi, L. Ning, Z. Wang, J. Chen, T. Sham, Y. Huang, Z. Qi, C. Li, Q. Tang, H. Liang, Zero-thermal quenching of Mn^{2+} red luminescence via efficient energy transfer from Eu^{2+} in $BaMgP_2O_7$, *Adv. Opt. Mater.* (2019) 1901187.
- [27] X. Zhang, J. Luo, Z. Sun, W. Zhou, Z. Wu, J. Zhang, Ultrahigh-energy-transfer efficiency and efficient Mn^{2+} red emission realized by structural confinement in $Ca_9LiMn(PO_4)_7$: Eu^{2+} , Tb^{3+} phosphor, *Inorg. Chem.* 59 (2020) 15050–15060.